Biofunctional Subwavelength Optical Waveguides for Biodetection

Donald J. Sirbuly,* Nicholas O. Fischer, Shih-Chieh J. Huang, Alexander B. Artyukhin, Jeffrey B.-H. Tok, Olgica Bakajin, and Aleksandr Noy*

Chemistry, Materials, Earth, and Life Sciences Directorate, Lawrence Livermore National Laboratory, 7000 East Avenue, Livermore, California 94550

ARTICLE

ABSTRACT We report a versatile biofunctional subwavelength photonic device platform for real-time detection of biological molecules. Our devices contain lipid bilayer membranes fused onto metal oxide nanowire waveguides stretched across polymeric flow channels. The lipid bilayers incorporating target receptors are submersed in the propagating evanescent field of the optical cavity. We show that the lipid bilayers in our devices are continuous, have very high mobile fraction, and are resistant to fouling. We also demonstrate that our platform allows rapid membrane exchange. Finally, we use this device to detect the hybridization of specific DNA target sequences in solution to complementary probe DNA strands anchored to the lipid bilayer. This evanescent wave sensing architecture holds great potential for portable, all-optical detection systems.

KEYWORDS: photonics · evanescent field · subwavelength · sensor · lipid bilayer · waveguide

Designing advanced optical components for biological diagnostics will require interfacing the cellular environments with photonic materials. Supported phospholipid bilayer membranes represent a versatile, robust, and increasingly common approach for achieving biological compatibility for materials surfaces.[1–3] Because of the central role the lipid bilayers play in a variety of important cellular processes,[4] such as molecular transport, signaling, and recognition, they provide almost limitless possibilities for integrating living biosystems with manmade materials and devices. For all-optical, chip-based biochemical sensing and analysis, lipid membranes represent a viable and highly versatile means for functionalizing an active sensing element with target receptors. Nonfouling properties of the lipid membrane also enable efficient rejection of nonspecific interactions.[1]

The ease of fabricating a continuous lipid membrane by vesicle fusion is well documented.[3,5,6] This process allows efficient formation of a bilayer on a wide variety of support materials,[3] geometries,[7] and curvatures[8] in a matter of seconds to minutes. It is also extremely flexible in producing membranes with various chemical compositions. For example, membranes containing charged phospholipids, glycolipids, and membrane-linked or membrane-embedded proteins can be created under virtually the same synthetic conditions.[9] These characteristics make lipid membranes an ideal environment for integration with subwavelength optical components.

The next generation of ultrasensitive optical biosensor strategies has to rely on materials and structures that can efficiently deliver photons to a small probing area. Recently, Craighead and co-workers demonstrated single-molecule spectroscopy using lipid-membrane-coated zero-mode waveguides.[10] Although volume confinements with the zero-mode waveguides can reach the zeptoliter (10^{-21} L) range, enabling single-molecule analysis at biological concentrations, the nonpropagating optical field makes simultaneous readouts and multiplexing difficult. High-aspect-ratio ($>10^3$), subwavelength semiconductor nanowires[11] represent an alternative class of materials that can support a propagating optical wave for spectroscopic analysis and can sustain single inputs for manifold analyzers. Tin dioxide (SnO_2) nanowires are one example of a one-dimensional (1D) semiconductor waveguide that has subwavelength rectangular cross-sections ranging from 100 to 400 nm. These dimensions allow up to 30% of the confined optical energy to travel outside the waveguide (see Materials and Experimental Methods section) in the surrounding cladding, penetrating up to ~160 nm beyond the waveguide surface before decaying to 10% of the power confined in the waveguide core. This property offers a uniquely efficient platform for designing miniaturized optical sensors. In fact, the optical power in the

*Address correspondence to sirbuly2@llnl.gov; noy1@llnl.gov.

Received for review September 10, 2007 and accepted January 17, 2008.

Published online February 7, 2008. 10.1021/nn700220b CCC: $40.75

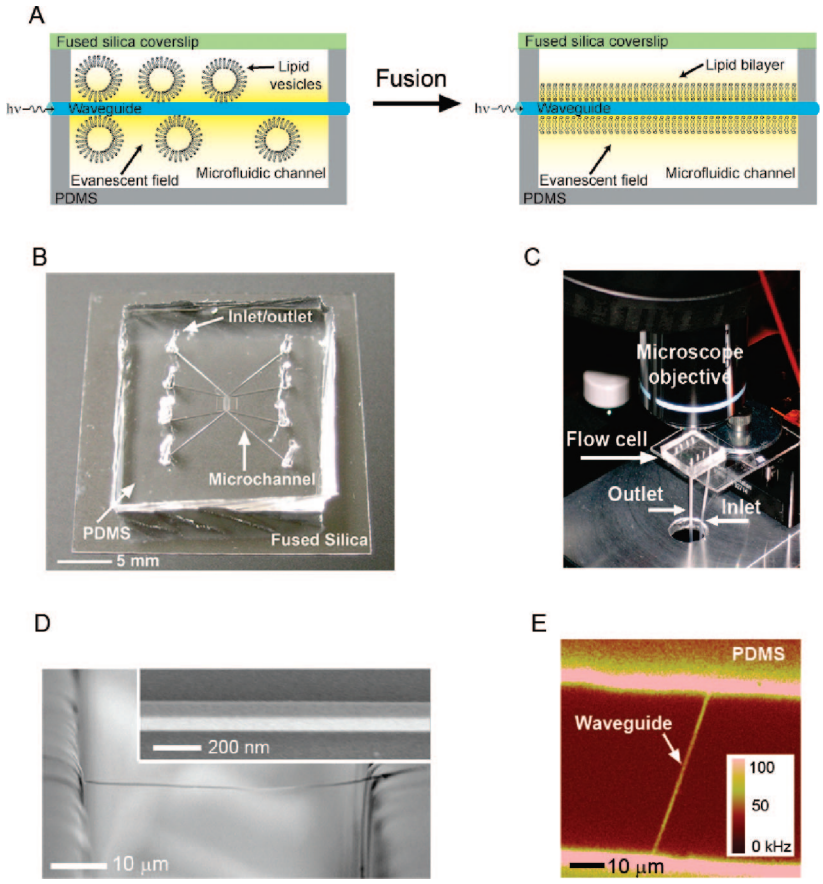

Figure 1. Schematic and layout of the microfluidic flow cell for bilayer formation. (A) Cartoon showing lipid vesicles adsorbing within the evanescent field of a subwavelength waveguide. Light is coupled into the waveguide and travels parallel to the wire axis. For the waveguide diameters used here, the exponentially decaying evanescent field penetrates ~140 nm into the liquid cladding before attenuating to 10% of the power confined in the waveguide core. After fusion of the lipid vesicle, a continuous, mobile lipid membrane coats the optical surface. Not shown is the bilayer that forms on the fused silica coverslip and PDMS channel. (B) Digital picture of a PDMS flow cell highlighting the microchannels, glass coverslip, and inlet/outlet holes. (C) Upright microscope setup for the flow cell. The elastomeric cell sits with its fused silica cover glass facing the microscope objective. (D) Scanning electron micrograph of a waveguide suspended over a microchannel. Inset: Zoom-in SEM image of the surface of a SnO_2 waveguide showing the rectangular geometry of the cavity. (E) Confocal optical image (80 × 80 μm scan) of a lipid-coated waveguide suspended across a PDMS microchannel. Here the fluorescence is generated by an excitation traveling perpendicular to the waveguide (not with the evanescent field of the waveguide).

evanescent field residing near the surface of these subwavelength optical cavities is sufficient to carry out complementary spectroscopic techniques, such as fluorescence, absorption, and surface-enhanced Raman spectroscopy (SERS), on femtoliter probe volumes.[12]

Here we describe a versatile generalized strategy for biocompatible functionalization of free-standing subwavelength SnO_2 waveguides integrated into a polymeric flow cell by assembling a fluid lipid membrane directly on the waveguide surface. Under slow flow conditions, lipid vesicles fuse on the waveguide surfaces within seconds to form freely mobile bilayers. Rapid cleaning (<5 s) of the waveguides and fast lipid exchange demonstrate the possibility of creating a robust and reusable optical sensing platform based on these nanowire waveguides. Finally, we show that these devices can function as biomolecular sensors by anchoring oligonucleotide strands within the lipid bilayer and observing real-time hybridization of complementary single-stranded DNA species. These results demonstrate the possibility of encoding nanophotonic materials for biochemical detection and lay the groundwork for all-optical monitoring of biological processes.

We chose to use single-crystalline SnO_2 nanowire waveguides as the subwavelength optical cavities because of their exceptional combination of optical, mechanical, and structural properties that enable simple device integration. SnO_2 is a wide-band-gap semiconductor (E_g = 3.6 eV, 344 nm) and a transparent metal oxide with a refractive index (n) of 2.1 (for visible wavelengths), making it ideal for optical confinement within the visible and near-ultraviolet frequency ranges.[13] The high index of refraction, compared to that of silica ($n \approx$ 1.45), allows light to be shuttled around an optical chip surrounded by silica or polymer fluidic channels without significantly increasing propagation losses. The strong optical confinement enables smaller fibers to be used and ultimately allows higher packing densities in photonic devices. Furthermore, for prototype device fabrication, the lengths and mechanical durability of the SnO_2 waveguides facilitate waveguide transfer to a secondary substrate or device. We use micromanipulation to transport the nanowires to an elastomeric flow cell made from poly(dimethylsiloxane) (PDMS) where the waveguides traverse across 50 μm wide × 25 μm deep channels. To provide optimal power in the evanescent field while maintaining diffraction-limited dimensions, we only used waveguides with diameters of ~150–200 nm. After the device is sealed with a fused silica coverslip, the waveguides lie suspended over the microchannel, approximately 5–10 μm from the glass substrate, thereby giving the analyte full access to the surface of the SnO_2 cavity (Figure 1A). The sealed devices formed a robust, small, and portable package (Figure 1B) that could be interrogated with a variety of optical techniques (Figure 1C).

1,2-Dioleoyl-*sn*-glycero-3-phosphocholine (DOPC) lipid vesicles containing 1% of the fluorescently labeled lipid marker 1-oleoyl-2-[6-[(7-nitro-2-1,3-benzoxadiazol-4-yl)amino]hexanoyl]-*sn*-glycero-3-phosphoethanolamine (NBDPE) rapidly fused with the waveguide surface (see Figure 3b), either when the lipid solution was dropped onto the waveguide surface or when it was pulled through the sealed microchannel

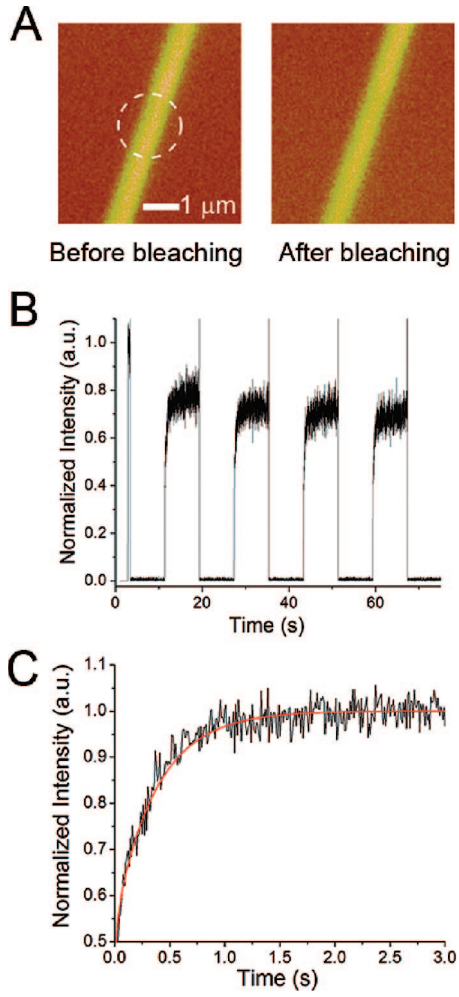

Figure 2. Fluorescence recovery after photobleaching (FRAP) data. (A) Two confocal optical images of a suspended waveguide before and after photobleaching. The lipid bilayer is comprised of DOPC molecules doped with 1% NBDPE (fluorescent lipid). The bleached area is denoted by the white dashed circle. (B) FRAP cycling of a bilayer coating a single SnO_2 waveguide. The bleach and read laser power densities were held fixed at 12 and 0.12 kW/cm^2, respectively. The sharp spike in counts before the bleach cycle is due to a short delay (~10 ms) between the shutter and electro-optic modulator. Even after five bleach cycles, the bilayers reached an average recovery of 75% the initial intensity. (C) A single FRAP trace (black curve) with a 1D diffusion model fit (red curve). The diffusion coefficients of the waveguide-supported DOPC lipid membranes consistently fell within 2×10^8–5×10^8 cm^2/s.

with the waveguide stretching across it. Optical images of the waveguide surface (Figure 1E, Figure 2A) show that this procedure produces continuous and uniform lipid coatings, while the optical spectrum (Supporting Information, Figure S1) confirms that the fluorescence visible in Figure 2 is coming from the dye-labeled lipid molecules.

A critical feature that defines a functional lipid membrane is the ability of individual lipid molecules to diffuse rapidly along the support surface within the bilayer plane. To test the continuity and determine the diffusivity of our membranes on the SnO_2 surface, we carried out fluorescence recovery after photobleaching (FRAP) experiments.[14] SnO_2 nanowire waveguides showed an average recovery of *ca.* 75% after photobleaching, even after multiple bleaching cycles (Figure 2B). The images in Figure 2A illustrate that only minimal fluorescence signal was lost from the bleaching area (~0.2 μm^2) after five cycles. We used a previously described 1D diffusion model[8] to determine the lipid mobility from the recovery kinetics. The model assumes that the focused laser spot uniformly bleaches all lipid molecules around the waveguide and that the recovery occurs only from directions parallel to the wire axis. As our waveguides are substantially longer than the bleaching spot size and characteristic diffusion length during bleaching, we can treat the unbleached areas of the cavities as large, inexhaustible lipid reservoirs. For the native SnO_2 surface-supported DOPC membranes, we obtain a diffusion constant of 2×10^8–5×10^8 cm^2/s, which is nearly identical to that of fluid bilayers absorbed to glass substrates.[15] This comparison demonstrates that lipid bilayers form very high quality coatings on the bare SnO_2 nanowire surfaces.

Exciting the lipid molecules with the evanescent field rather than directly with the laser spot suppresses the background fluorescence (Figure 3A) and eliminates the need for using a clean, uncoated cover glass and scanning microscope. The kinetic curve of the lipid bilayer fusion (Figure 3B) shows that, within 5 s (at a flow rate of ~10 mL/h), the fluorescence intensity reaches a maximum and stabilizes as pure buffer removes excess lipid vesicles from the waveguide. The optical images of the fusion process show a slight darkening near the center of the waveguide. Since the optical cavities reside only a few micrometers below the fused silica cover glass, they can bend upward and stick to the glass. This causes a weaker signal due to fewer lipid molecules adhering between the waveguide and cavity. The SnO_2 waveguides are extremely flexible (note the slight curvature in the image plane), and a strong liquid pulse can release the waveguide from the glass to allow complete bilayer coverage (see Figure 3C).

The use of amphiphilic solvents such as detergents or alcohols is a reliable means of removing the lipid bilayer from the waveguide and restoring the initial optical surface. We were able to remove the lipid bilayers from the waveguide by passing a short pulse of pure ethanol through the fluid cell (Figure 3C). The alcohol quickly desorbs the lipid membrane in <1 s and returns the fluorescence intensity to background levels. Using this protocol, membranes can be rapidly exchanged with a solution pulse train consisting of lipid vesicles, pure buffer, and alcohol. This membrane exchange procedure is robust and can be repeated multiple times (Figure 3D) without any degradation of the waveguide device. It is important to note that the chemical composition of the membranes can be changed during these exchanges, provided that the chosen lipid molecules form stable supported lipid bilayers (*via* vesicle fusion)

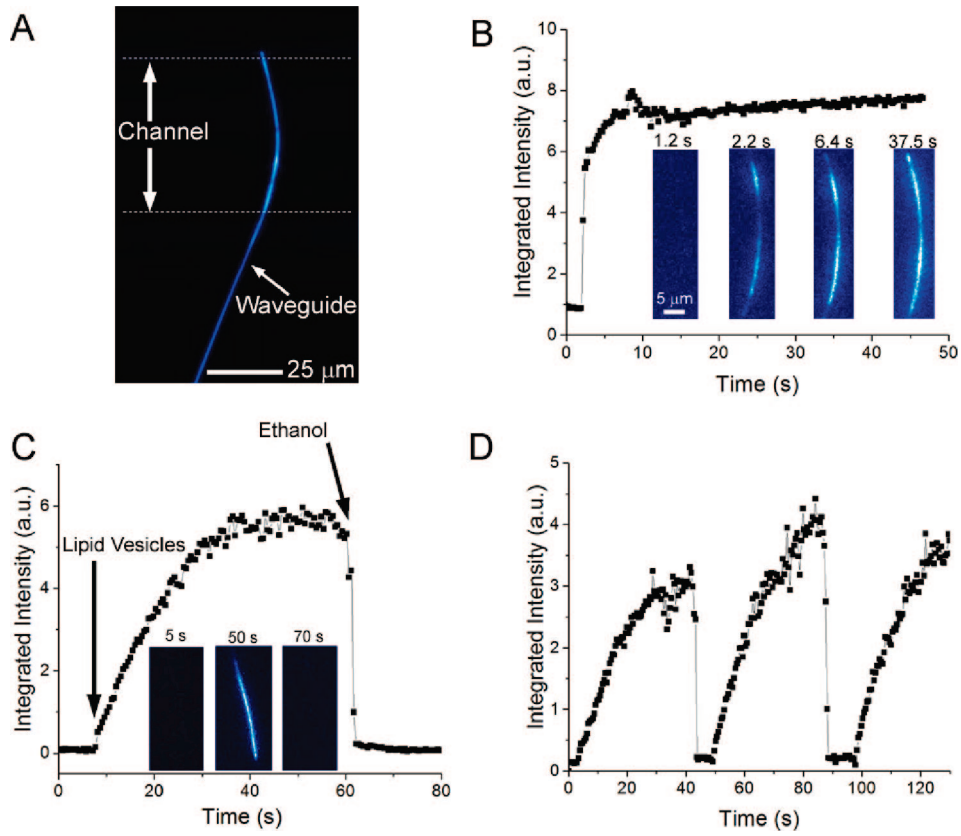

Figure 3. Bilayer fusion and membrane exchange. (A) Dark-field optical image of a subwavelength waveguide embedded in a PDMS flow cell. Monochromatic light (442 nm) is launched into the waveguides at the bottom end terminal (outside the field of view). (B) Intensity time course taken from the short waveguide segment traversing the microchannel in panel A as DOPC/NBDPE (99%/1%) lipid vesicles (in 10 mM Tris-HCl, pH 8) fuse on the SnO_2 surface. The optical micrographs show the lipid coverage at discrete times during the fusion process. The evanescent field is exciting the NBDPE lipid molecules within the bilayer. (C) Intensity time course of vesicle fusion (<1 mL/h pulling rate) followed by membrane removal with an alcohol (ethanol) liquid pulse. The optical micrographs verify a fused bilayer (time = 50 s) and a membrane-free waveguide after cleaning (time = 70 s). (D) Intensity time course of multiple lipid−pure solvent−ethanol pulses. Membranes can be rapidly exchanged using sequential liquid pulse trains of lipid and an amphiphilic solvent.

on the tin dioxide surface. Strong acids (*e.g.*, aqua regia solution) can also be used to strip off any contaminants residing on the optical surface after repetitive experimental runs. We have repeatedly cleaned the SnO_2 surface with a solution containing 1 part concentrated hydrochloric and nitric acids (ratio of 1:3) to 3 parts water without noticing any decrease in the optical performance of the waveguide.

Lipid membranes are excellent scaffolds for embedding or tethering biological molecules using anchors such as membrane proteins or modified lipids. We used this approach to anchor a short DNA oligonucleotide (21-nucleotide recognition sequence, T_5 spacer) modified with a 3′ cholesterol tail to the bilayer.[16] It is important to note that we did not observe any fragmentation of the DNA strands during vesicle preparation (Supporting Information, Figure S2); therefore, we assume that, after the insertion of the cholesterol tail into the hydrophobic core of the lipid bilayer, the DNA protrudes into the hydrophilic vesicle core or into the surrounding aqueous medium outside the vesicle (Figure 4A). Fluorescence imaging using a nucleic acid stain, YOYO-1, showed that, after the vesicles fused the waveguide, the single-stranded (ss) DNA molecules remain anchored to the membrane and form a continuous bilayer coating on the waveguide (Figure 4B). We have also successfully inserted probe ssDNA into a pure DOPC membrane (no DNA) on the waveguide by flowing cholesterol-tagged DNA into the channel after membrane fusion (data not shown). It is clear from the confocal fluorescent images in Figure 4C that the recovery is much slower than for the dye-tagged lipids described above and shows a measurable decrease in fluorescence intensity over the bleached section after approximately 5 min (Figure 4C, inset image 3). The FRAP data verifies a slower diffusion constant of 0.1×10^{-8}–0.2×10^{-8} cm^2/s, which is an order of magnitude slower than the diffusion constant measured for the NBDPE-doped DOPC membranes. A slower diffusion coefficient is expected since we are monitoring the cholesterol-modified DNA molecules, which have a larger size and charge than the dye-labeled lipid molecules. More importantly, however, the FRAP data and fluorescent images confirm that our oligonucleotide-doped bilayers are continuous and mobile.

To demonstrate the biomolecular sensing capabilities of our device platform, we monitored real-time hybridization of two complementary 21-base-pair ssDNA sequences. One of the sequences was anchored to the surface of the waveguide-supported bilayer (probe ssDNA) while free target DNA (cDNA) was flowed through the sealed microchannel. The DNA used in these experiments was labeled with PicoGreen dye, which is an excellent dye for differentiating between single- and double-stranded DNA (dsDNA) due to its large fluorescence enhancement upon binding to dsDNA. In free solution (no lipids present), the dye shows ~30× and ~100× enhancement in fluorescence over the free dye when binding to ssDNA and dsDNA, respectively (Sup-

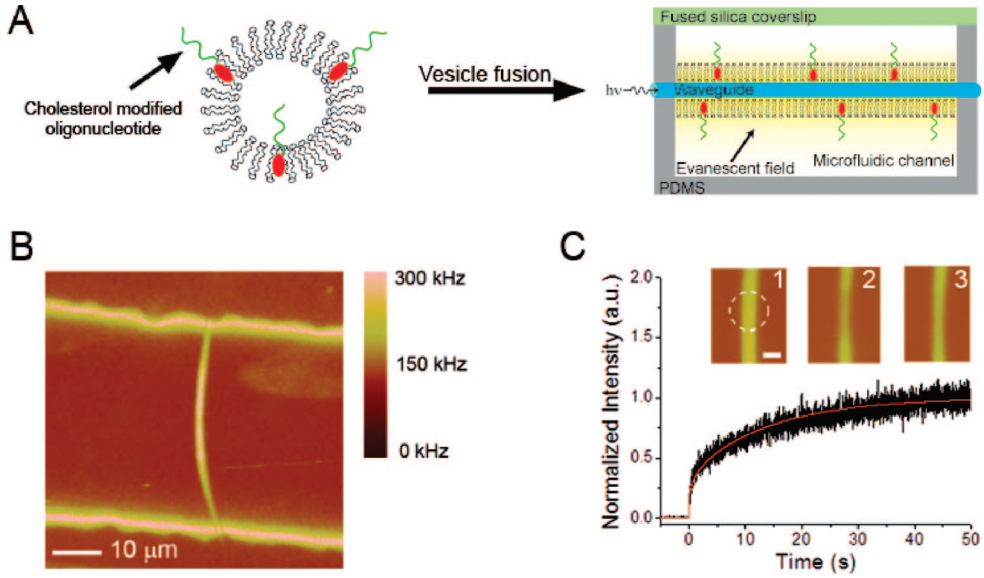

Figure 4. Oligonucleotide-doped lipid membranes. (A) Schematic of a DNA-doped vesicle and the resulting bilayer. It is possible for some of the strands to point their 5′ ends toward the waveguide instead of into the microchannel (not drawn). Note that the DNA strands were drawn with a stretched orientation, rather than the more likely coiled-up configuration, for clarity only. (B) Confocal fluorescence image (80 × 80 μm scan) of a YOYO-1-labeled lipid bilayer doped with the probe ss-DNA (1% molar ratio doping). The slight bending of the waveguide is a result of the transfer process. The waveguides are extremely flexible (*i.e.*, mechanically) and can sustain high curvature without disrupting bilayer formation. (C) FRAP trace of the DNA-doped lipid bilayer showing an order of magnitude slower diffusion ($D = 0.1 \times 10^{-8}$–0.2×10^{-8} cm^2/s) compared to that of the DOPC/NBDPE membranes. The raw data and 1D diffusion model fit are shown in black and red, respectively. Inset: Sequential confocal images of the same waveguide in panel B, (1) before photobleaching, (2) ~2 min post-photobleaching, and (3) ~5 min post-photobleaching. The white dashed circle denotes the approximate position of the laser beam. Scale bar is 500 nm.

porting Information, Figure S3a). Similar enhancements in the fluorescence were observed from the oligonucleotide-doped lipid vesicles, displaying 3× increase in intensity when the cDNA was injected into the solution (Figure 5B). The hybridization on the lipid vesicle surface in free solution is very rapid: over 85% of the annealing occurs within the first minute and no additional dye is required to label the hybridized DNA pairs. Thus, sensing in the microfluidic devices is simplified by eliminating the need to flow free reporting dye into the flow cell during hybridization. We can perform the sensing experiments by tagging only the DNA probe sequence anchored to the lipid bilayer.

Using the evanescent field to detect hybridization allows us to monitor only those photons that are emitted from the dye molecules residing near the surface of the waveguide (Figure 5A). After the probe DNA-doped bilayer forms on the waveguide, the fluorescence signal reaches a steady state (Figure 5C, time courses). However, once the front of the solution pulse containing target DNA encounters the waveguide, the intensity increases approximately 1.8–2.5× above the bilayer level, indicating that DNA hybridization has occurred. In contrast, no enhancement occurred in solution when mismatched target DNA was added to the probe DNA (Supporting Information, Figure S3b). There is a slight reduction in the intensity level after hybridization, which could indicate a removal of residual dsDNA molecules (*i.e.*, a small fraction of dsDNA that is not inserted into the bilayer). In addition, there may be slight conformational changes in the DNA as it hybridizes (*i.e.*, from coiled ssDNA to extended dsDNA), causing the fluorescent probes to move farther (*ca.* 2–4 nm) from the waveguide surface. This distance change, however, is too small (and too rapid) to cause the observed decay in optical signal, even though the power in the evanescent field is decaying exponentially. The result of such a change in DNA length would likely just lower (<3%) the peak intensity after hybridization and not cause the delayed drop observed in the data

In general, the intensity enhancements observed for DNA hybridization on the lipid-coated waveguides were *ca.* 25% smaller than the intensity enhancement in solution hybridization experiments. One explanation is that the amount of available dye is reduced in the waveguide experiment. Hybridization of the DNA in free solution occurs in the presence of excess PicoGreen, whereas in the waveguide experiments the only accessible PicoGreen dye molecules for the target cDNA are those complexed with the probe ssDNA or the small fraction of dye molecules that remains nonspecifically bound to the bilayer surface. Since the hybridization event can conceivably displace a portion of the bound PicoGreen, the overall amount of dye available before and after hybridization is reduced, resulting in a lower intensity enhancement. It is also possible that labeled probe DNA sandwiched between the waveguide and inner leaflet of the bilayer is not accessible to the target DNA. In this configuration, the

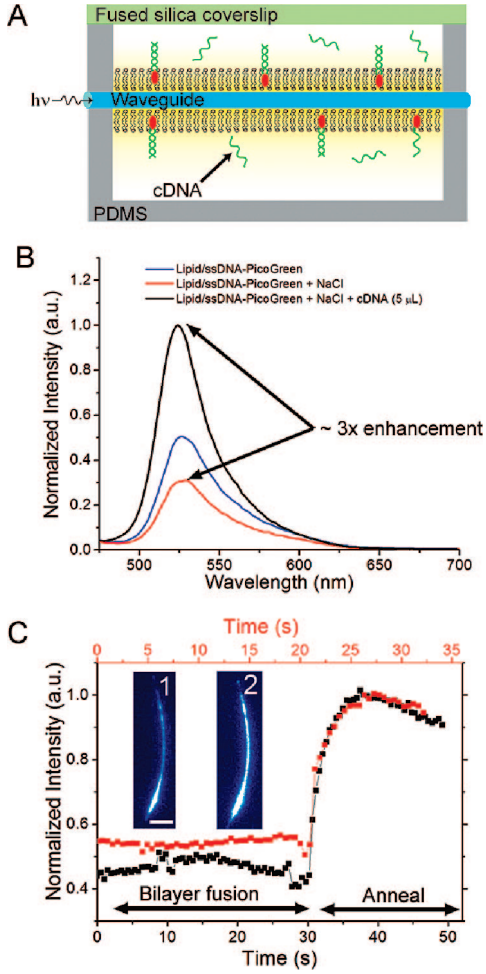

Figure 5. Real-time detection of DNA hybridization. (A) Schematic of annealed DNA anchored by the cholesterol-modified probe strands. The hybridization is monitored by the fluorescence generated by the evanescent field of the optical waveguide. (B) Fluorometry data of DNA-doped vesicles in free solution (TBS, pH 8). The data show an ~40% decrease in intensity upon salt addition and ~300% increase after cDNA is injected into the solution. The decrease is well documented for PicoGreen in NaCl solutions. Spectra are normalized so that the cDNA peak is 1. (C) Two intensity time courses showing hybridization of the target cDNA strands with the probe DNA anchored in the supported lipid membrane. The top (red) and bottom (black) time axes correspond to the red and black traces, respectively. The flow rate was kept below 1 mL/h for ~20 s prior to annealing to ensure complete bilayer formation and to remove unanchored probe DNA. There is an average of 1.8–2.5× increase in the fluorescence intensity after the target strand encounters the lipid bilayer. Time courses are normalized so that the peak integrated intensity is 1. The optical images are single snapshots taken from a time course (1) during bilayer formation and (2) after annealing. Scale bar is 10 μm.

overall enhancement will be lower, as only the fraction of the DNA molecules properly positioned at the solvent-exposed face of the bilayer are contributing to the fluorescent signal. Finally, as described earlier, the DNA conformational changes that occur during hybridization could lower the overall enhancement since dsDNA, and associated fluorophores, will extend farther from the waveguide surface. We have performed extensive tests to verify that hybridization was occurring with bilayer-supported probe strands, rather than nonspecific bound dsDNA interacting with an uncoated waveguide *via* electrostatic interactions. Flowing PicoGreen-labeled dsDNA over a lipid-free waveguide produced only a weak fluorescent signal with intensity comparable to that of the ssDNA-doped bilayer (data not shown).

In conclusion, we have developed a versatile nanoscale spectroscopic platform that interfaces subwavelength optical waveguides with functional biological membranes. Vesicle fusion produces continuous and mobile lipid membranes situated directly within the propagating evanescent field of a metal oxide nanowire optical cavity. Membranes assembled on the nanowires integrated into polymeric flow cells can be rapidly exchanged by alternating short pulses of organic solvent and vesicle solution. This protocol allows sub-10-s chemical compositional changes to the optical surface. Finally, we showed that the waveguides incorporating ssDNA molecules anchored to the lipid bilayer surface can be used for DNA detection. In these experiments, hybridization of the complementary target DNA strand to the probe DNA on the waveguide, in the presence of a DNA-sensitive dye, produced a real-time enhancement of the dye fluorescence. Although we demonstrated the detection technique with micromolar DNA concentrations, improvements in collection geometry, background reduction, use of small light-scattering nanoparticles, and experimentation with alternate detection schemes (*e.g.*, interferometry, light scattering, *etc.*) should enable single-molecule detection that can capitalize on the high-throughput nature of microfluidic devices.

Our results open up several important directions for real-time chip-based optical detection of biological molecules. Nanoscale photonic scaffolds will be a crucial component for the development of miniaturized multiplexed optical sensors which require individual transducers to be encoded with distinct chemical specificity. The subfemtoliter probe volumes, reusability, and ability to use various optical sensing modalities make our biofunctional waveguides an ideal portable photonic platform for biomolecular screening, sensing, and *in situ* medical diagnostics.

MATERIALS AND EXPERIMENTAL METHODS

SnO_2 Waveguide Synthesis. Tin dioxide (SnO_2) optical waveguides were synthesized by thermal vaporization of tin monoxide powders in the presence of trace amounts of oxygen, similar to previous accounts.[13,17] Briefly, tin monoxide powder (99.9%, Alfa Aesar) was placed in an alumina boat and heated in an alumina tube furnace (~1085 °C), evacuated to 300 mTorr under a 25 sccm flow of argon. After an ~1 h growth period, the waveguides were dry-transferred from the alumina boat surface to a clean silica surface.

Optical Microscopy. Optical characterization of the sealed and unsealed microfluidic devices was performed with an upright dark-field microscope (see Figure 1C) and inverted laser scanning confocal microscope, respectively. Fluorescence signal was captured with the dark-field microscope using a 50× (Nikon, NA 0.55) objective operating in reflection mode. Signal was either imaged with an EMCCD camera (Andor Technology) or routed to a fiber-optic-coupled spectrometer (Roper Scientific). A continuous-wave helium−cadmium laser (Kimmon Electric) provided linearly polarized ultraviolet (325 nm) or blue (442 nm) radiation for the dark-field microscope. The laser beam was focused to an ~50-μm-diameter spot onto the sample at an approximate angle of 45° relative to the sample lying horizontal under the microscope objective. Power densities at the sample ranged from 8 to 25 W/cm^2 for the 442 nm line and from 230 to 270 W/cm^2 for the 325 nm line but were held fixed during a single experiment.

The 325 nm laser line was used to determine the waveguiding properties of the SnO_2 nanowire by generating its broad (380–700 nm), featureless defect emission at one end facet and observing the emission color at the opposing end. According to the waveguide parameter expression $\lambda_c = (d_e\pi(n_{co}^2 - n_{ci}^2)^{1/2})/2.405$ for a cylindrical optical cavity,[18] the single-mode cutoff wavelength (λ_c) relates directly to the single-mode cutoff diameter (d_c) of the waveguide and can be used to estimate cross-sectional dimensions of the SnO_2 cavity. In general, only waveguides with $\lambda_c \leq 600$ nm were used in the devices, which corresponds to $d_c \leq 250$ nm, in good agreement with the actual sizes of the nanowires used here. The fraction of fundamental modal power (η) in the core of a cylindrical waveguide can be approximated by[18]

$$\eta = 1 - \frac{5.784 \exp{-(2/V)}}{V^3}$$

where $V = (\pi d(n_{co}^2 - n_{cl}^2)^{1/2})/\lambda$. Therefore, the dimensions of the nanowire waveguides carry ~15–30% of the guided power outside the cavity in the evanescent field.

The 442 nm line was used for the evanescent sensing experiments by focusing the laser light on the end facet of the waveguide. Fluorescence generated within the evanescent field was collected by the objective centered over the microfluidic channel and directed to the spectrometer or camera.

The inverted laser scanning confocal microscope imaged the unsealed devices using the 488 nn line (linearly polarized) of an Ar^+ laser (Spectra-Physics) attenuated to ~120 W/cm^2 at the sample. The excitation beam was focused to *ca.* 1 μm diameter with a 60× water immersion objective (Nikon, NA 1.20). The sample was raster scanned across the beam with a nanopositioning stage (Physik Instrumente) controlled by commercially available scanning electronics (Digital Instruments). After the laser light was removed from the fluorescence, the signal was routed to an avalanche photodiode (APD) and processed by a photon-counting board integrated with the scanning electronics.

Device Fabrication. Polymeric flow cells were cast from poly(dimethylsiloxane) (PDMS) using a silicon master fabricated using standard lithography techniques. There are four channels running parallel to each other, with dimensions 1.25 mm long × 50 μm wide × 25 μm deep, spaced 50 μm apart. After the elastomer stamp was cured, a thin (~5–10 μm) wet PDMS layer was placed on the structured side of the stamp. This was achieved by spinning (6000 rpm) uncured PDMS on a glass coverslip and touching the structured side of the stamp to the wet layer. Waveguides optically screened according to the procedure described above were then transferred to the stamps using a three-axis micromanipulator (Marzhauser Wetzlar) equipped with an etched tungsten probe. Orientation of the cavities was controlled so that the waveguides traversed across the channels, leaving one of the end facets accessible for coupling laser light. Devices were sealed for the flow experiments by curing the wet layer after a fused silica coverslip was placed on the structured side of the stamp. Curing without a coverslip prepared the sample for confocal fluorescence microscopy. Since the lipid membranes fuse over the entire microchannel, including the glass coverslip, confocal imaging could only be performed with an unsealed device.

Lipid Bilayer Preparation. Unilamellar fluorescent lipid vesicles were prepared *via* tip probe sonication using a mixture of 1,2-dioleoyl-*sn*-glycero-3-phosphocholine (DOPC) lipid and a dye-tagged lipid, 1-oleoyl-2-[6-[(7-nitro-2-1,3-benzoxadiazol-4-yl)amino]hexanoyl]-*sn*-glycero-3-phosphoethanolamine (18:1–06:0 NBDPE) purchased from Avanti Polar Lipids. Appropriate volumes of the lipid stock solution (in chloroform) were transferred to a sample vial to evaporate the chloroform, giving a DOPC/NBDPE molar ratio of 99.0:1.0. After water (or Tris-HCl buffer, see below) was added to the dried lipids, a lipid concentration of 0.3 mg/mL (0.1 mg/mL for the sealed devices) was achieved. The mixtures were tip sonicated at 9 W for ~1 min at room temperature prior to use. Membrane formation on the waveguides was initiated on the sealed devices by pulling (flow rates of 1–10 mL/h) the vesicles over the waveguides for ~1 min (fusion occurred within seconds) and then flushing the channels with pure buffer to remove excess lipid. For the unsealed devices, a small droplet (~5 μL) of lipid vesicle solution was placed on the channel side of the stamp for ~5–10 min and then washed with copious amounts of water before a clean fused silica cover glass was placed over the microchannels.

Fluorescence Recovery after Photobleaching. Fluorescence recovery after photobleaching (FRAP) experiments were achieved by parking the laser scanning confocal microscope over the center portion of a suspended waveguide. The laser beam was attenuated at a rate faster than the recovery kinetics using an optical train consisting of an electro-optic modulator (EOM, Conoptics) and a linear polarizer. The laser intensity was modulated between the bleach (12 kW/cm^2) and read (120 W/cm^2) powers using a function generator (coupled to the EOM) outputting a 62.5 mHz square wave (8 s bleach and read cycles) with an amplitude of 2 V_{p-p}. The function generator was synced to an electric shutter so that the APD was blocked during the bleach period and open during the read block. FRAP traces were generated by inputting the raw counts from the APD into a counting board (National Instruments). Fits to the recovery curves were performed using the unbinned data from the counter.

DNA Anchoring and Sensing. Single-stranded DNA (ssDNA) was anchored in the lipid bilayer by resuspending the dried DOPC lipids in a solution of 10 mM tris(hydroxymethyl)aminomethane hydrochloride (Tris-HCl, pH 8.0) containing the cholesterol-modified oligonucleotides (Integrated DNA Technologies, Inc.). Unless specified, the molar ratio of lipid/DNA was 99.0:1.0. The cholesterol modification was placed at the 3′ end of a 26-nucleotide oligonucleotide and featured a tetra(ethyleneglycol) (TEG) linker. The FRAP data were recorded using a cholesterol TEG linker on the 5′ end of an 18-base oligonucleotide (5′-CholTEG/AGG CGC TGC CAG CGT CAT C-3′). The final lipid concentration of the solution was adjusted to 0.1 mg/mL with additional Tris-HCl, keeping the pH at 8.0. Tip probe sonication procedures similar to those described above were carried out on the DNA-doped lipid vesicles to create unilamellar vesicles. Gel electrophoresis was used to verify that there was no fragmentation of the DNA after sonication (see Supporting Information, Figure S2). Procedures identical to those described above were utilized to fuse the DNA-doped lipid vesicles on the waveguides in the sealed and unsealed devices. We labeled the anchored single strands of DNA, after bilayer formation, for the confocal (unsealed devices) and annealing studies (sealed devices) with YOYO-1 (Invitrogen) and PicoGreen (Invitrogen), respectively.

For the real-time annealing experiments, Tris-buffered saline (TBS; 10 mM Tris-HCl, pH 8.0, 50 mM NaCl) was used for hybridization and washing. After the PicoGreen-labeled vesicles, suspended in 10 mM Tris-HCl, were fused, a liquid pulse train was pulled through the microchannel in the following order: lipid vesicles, TBS buffer, complementary target DNA (cDNA), TBS buffer. The cDNA solution had a DNA concentration of 15 μM in TBS. Fluorescence generated by the evanescent field was monitored with a camera running at ~2 Hz and capturing 200 sequential 512 × 512 pixel images. The sequences for the oligo-

nucleotides were 5′-TCC TGT GTC GAA TTG TTA TCC TTT TT/3CholTEG/-3′ (probe DNA) and 5′-GGA TAA CAA TTC GAC ACA GGA-3′ (target DNA).

Acknowledgment. D.J.S. acknowledges the Harold C. Graboske Jr. Fellowship from LLNL. N.O.F. acknowledges the CMLS Directorate Fellowship from LLNL. S.-C.J.H. and A.B.A. acknowledge support from the SEGRF fellowship at LLNL. A.N. acknowledges LLNL LDRD program funding. We would like to thank Yinmin Wang and Jim Ferreira for their help in capturing SEM images. This work was performed under the auspices of the U.S. Department of Energy by Lawrence Livermore National Laboratory under Contract DE-AC52-07NA27344.

Supporting Information Available: Figure S1, fluorescence spectrum of NBDPE generated by evanescent field; Figure S2, gel electrophoresis of sonicated and unsonicated oligonucleotides; and Figure S3, fluorometry data of PicoGreen. This material is available free of charge *via* the Internet at http://pubs.acs.org.

REFERENCES AND NOTES

1. Katsaras, J.; Gutberlet, T. *Lipid Bilayers: Structure and Interactions*; Springer-Verlag: Berlin, 2001; p 312.
2. Tien, H. T.; Ottova-Leitmannova, A. L. *Planar Lipid Bilayers (BLMs) and Their Applications*; Elsevier Science: Amsterdam, 2003; p 1043.
3. Sackmann, E. Supported Membranes: Scientific and Practical Applications. *Science* **1996**, *271*, 43–48.
4. Yeagle, P. L. *The Structure of Biological Membranes*; CRC Press: Boca Raton, FL, 2004.
5. Tamm, L. K.; McConnell, H. M. Supported Phospholipid-Bilayers. *Biophys. J.* **1985**, *47*, 105–113.
6. Evans, E. A. Analysis of Adhesion of Large Vesicles to Surfaces. *Biophys. J.* **1980**, *31*, 425–431.
7. Groves, J. T.; Ulman, N.; Boxer, S. G. Micropatterning Fluid Lipid Bilayers on Solid Supports. *Science* **1997**, *275*, 651–653.
8. Artyukhin, A. B.; Shestakov, A. I.; Harper, J.; Bakajin, O.; Stroeve, P.; Noy, A. Functional One-Dimensional Lipid Bilayers on Carbon Nanotube Templates. *J. Am. Chem. Soc.* **2005**, *127*, 7538–7542.
9. Groves, J. T. Membrane Array Technology for Drug Discovery. *Curr. Opin. Drug Discovery Dev.* **2002**, *5*, 606–612.
10. Samiee, K. T.; Moran-Mirabal, J. M.; Cheung, Y. K.; Craighead, H. G. Zero Mode Waveguides for Single-Molecule Spectroscopy on Lipid Membranes. *Biophys. J.* **2006**, *90*, 3288–3299.
11. Sirbuly, D. J.; Law, M.; Yan, H. Q.; Yang, P. D. Semiconductor Nanowires for Subwavelength Photonics Integration. *J. Phys. Chem. B* **2005**, *109*, 15190–15213.
12. Sirbuly, D. J.; Tao, A.; Law, M.; Fan, R.; Yang, P. D. Multifunctional Nanowire Evanescent Wave Optical Sensors. *Adv. Mater.* **2007**, *19*, 61–66.
13. Sirbuly, D. J.; Law, M.; Johnson, J. C.; Goldberger, J.; Saykally, R. J.; Yang, P. D. Nanoribbon Waveguides for Subwavelength Photonics Integration. *Science* **2004**, *305*, 1269–1273.
14. Axelrod, D.; Koppel, D. E.; Schlessinger, J.; Elson, E.; Webb, W. W. Mobility Measurement by Analysis of Fluorescence Photobleaching Recovery Kinetics. *Biophys. J.* **1976**, *16*, 1055–1069.
15. Tocanne, J. F.; Dupoucezanne, L.; Lopez, A. Lateral Diffusion of Lipids in Model and Natural Membranes. *Prog. Lipid Res.* **1994**, *33*, 203–237.
16. Benkoski, J. J.; Hook, F. Lateral Mobility of Tethered Vesicle−DNA Assemblies. *J. Phys. Chem. B* **2005**, *109*, 9773–9779.
17. Pan, Z. W.; Dai, Z. R.; Wang, Z. L. Nanobelts of Semiconducting Oxides. *Science* **2001**, *291*, 1947–1949.
18. Snyder, A. W.; Love, J. D. *Optical Waveguide Theory*; Chapman and Hall: London, 1983.